Mechanics Research Communications 83 (2017) 53–57

Contents lists available at ScienceDirect

Mechanics Research Communications

journal homepage: www.elsevier.com/locate/mechrescom

# Analytical modeling of constricted channel flow

Annemie Van Hirtum

*GIPSA-lab, CNRS UMR 5216, Grenoble Alpes University, 38000 Grenoble, France*

ARTICLE INFO

*Article history:*
Received 25 November 2016
Accepted 15 May 2017
Available online 24 May 2017

*Keywords:*
Laminar flow
Cross-section shape
Viscous boundary layer
Physiological flow

ABSTRACT

Analytical flow models are frequently applied when describing constricted channel flow at low and moderate Reynolds numbers. A common assumption underlying such flow models is two-dimensional or axi-symmetrical flow. In this work, two analytical model approaches are formulated in order to overcome this assumption in the case of naturally occurring channel flows for which the assumption might be critiqued. Advantages and flaws of both model approaches are discussed and their outcome is compared with experimental data.

© 2017 Elsevier Ltd. All rights reserved.

## 1. Introduction

Many applications rely on simplified laminar models to obtain an estimation of quasi-steady flow through constricted channels at a low computational cost. For low or moderate Reynolds numbers, viscous flow effects, which are known to depend on the cross-section shape [1,2], potentially affect the flow field. Nevertheless, common simplified models often rely on the assumption of two-dimensional or axi-symmetrical flow so that the cross-section shape is neglected. Imaging studies of naturally occurring constricted channel flows, such as physiological flow through blood vessels or airways, revealed a large variation of channel's cross-section shapes so that the assumption of two-dimensional (2D) or axi-symmetrical flow can be questioned for these applications [3]. In the following, two analytical flow models are considered which account for the cross-section shape of the constricted channel portion so that both result in 'quasi-three-dimensional'(quasi-3D) flow models. The first model (boundary layer model) makes the assumption of developing boundary layers whereas the second model (viscous model) relies on the asymptotic case of fully developed boundary layers.

## 2. Constricted channel flow

Pressure driven quasi-steady flow through a constricted channel (Fig. 1) is considered. A uniform circular channel (area $A_0$) envelops a constricted portion with minimum constriction (area $A_c$, length $L_c$, hydraulic diameter $D = 4A_c/\mathcal{P}$ with $\mathcal{P}$ the wetted perimeter) for which viscous effects can not be neglected. All corners are rounded (radius $r_a$). Flow is then generated by imposing upstream pressure $P_0$ so that the total driving pressure difference yields $\Delta P = P_0 - P_d$ with downstream pressure $P_d = 0$. Jet formation occurs near the downstream end of the constricted region ($x_s$) where the flow separates from the channel wall. The pressure distribution $P(x, t)$ along the constricted channel portion ($x_0 \leq x_2$) is sought for a known value of upstream pressure $P_0$.

Experimental data are obtained as described in [4]. Concretely, upstream pressure $P_0$, pressure $P_1$ at the middle of the constriction ($x/L_c = 0.5$) and volume flow velocity $\Phi$ are measured. In addition, spatial velocity profiles $u$ are measured along (longitudinal – $u(x)$) and perpendicular (spanwise – $u(y)$) to the main flow direction. Mean values are considered which are derived on 5 s of steady signal for the measured pressure signal $P(t)$ and volume flow rate $\Phi(t)$ and on 40 s for velocity $u(t)$.

## 3. Quasi-3D analytical laminar flow modeling

Low or moderate Reynolds number quasi-steady airflow (kinematic viscosity $\nu = 1.5 \times 10^{-5}\,\mathrm{m^2/s}$ and density $\rho = 1.2\,\mathrm{kg/m^3}$) is considered so that the flow within the constriction is assumed laminar and incompressible. The no-slip boundary condition is applied on the rigid channel walls. Volume flow velocity $\Phi$ is conserved so that $d\Phi/dx = 0$. Two cases are considered based on the ratio of constriction length to the entrance length of the constriction required to obtain fully developed viscous flow [1,2]. In the first case (Section 3.1), $L_c$ is short or comparable to the entrance length of the constricted portion so that viscous boundary layers develop within the constriction. Downstream from the constriction pressure recovery due to flow mixing is accounted for so that the expanding jet

*E-mail address:* annemie.vanhirtum@grenoble-inp.fr

http://dx.doi.org/10.1016/j.mechrescom.2017.05.006
0093-6413/© 2017 Elsevier Ltd. All rights reserved.

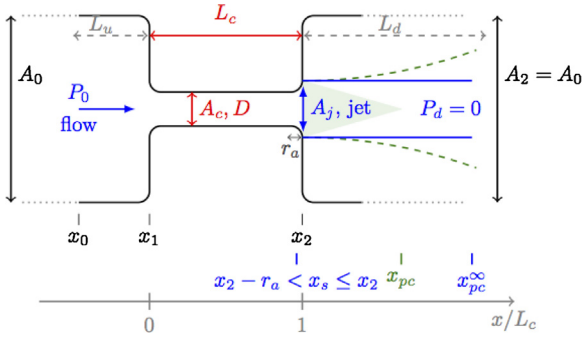


**Fig. 1.** Illustration of pressure driven flow through a uniform circular channel (area $A_0$) enveloping a constricted portion (area $A_c$, hydraulic diameter $D$ and length $L_c$). Sharp edges are rounded (radius $r_a$). Main streamwise direction $x$, pressure upstream from the constriction $P_0$, pressure downstream from the constriction $P_d$, flow separation position $x_s$, upstream unconstricted channel portion length ($L_u$) and downstream unconstricted channel portion length ($L_d$) are indicated. A non-expanding stable straight jet (full lines) with infinite potential core extent $x_{pc}^{\infty}$ and a developing jet (dashed curved lines) with finite potential core extent $x_{pc}$ (shaded area) are depicted.

has a finite potential core $x_{pc}$ (Fig. 1). In the second case (Section 3.2), $L_c$ is long compared to the entrance length of the constricted portion so that fully developed boundary layers are accounted for. Flow separation is discussed in Section 3.3.

### 3.1. Boundary layer model

A simple boundary layer flow model is proposed accounting for a developing boundary layer enveloping the core flow region. Pressure recovery due to flow mixing of the jet issued from the constriction with the surrounding fluid downstream from the constriction is accounted for using conservation of mass and momentum over the mixing region:

$$u_j A_j = u_2 A_2, \tag{1}$$

$$\rho u_2^2 A_2 = P_j A_2 + \rho A_j u_j^2, \tag{2}$$

where subindex $j$ and 2 indicate respectively the jet region (cross-sectional area $A_j$, velocity $u_j$ and pressure $P_j$) and the region downstream from the mixing zone (cross-sectional area $A_2 = A_0$, velocity $u_2$ and pressure $P_2 = P_d = 0$). The jet cross-sectional area $A_j$ is given as

$$\frac{A_j}{A_c} = \left(1 - \frac{2\delta_1}{D}\right)^2 \quad \text{or} \quad \frac{A_j}{A_c} \approx 1 - \frac{4\delta_1}{D} \quad \text{since} \quad \frac{2\delta_1}{D} < 1, \tag{3}$$

with $\delta_1$ the displacement thickness of the boundary layer approximated as the value for a flat plate of length $L_c$ associated with a Blasius velocity profile [2]:

$$\delta_1 \approx 1.7\sqrt{\frac{L_c D}{Re_{ref}}}, \tag{4}$$

where reference Reynolds number $Re_{ref} = \frac{D u_{ref}}{\nu}$ is defined using hydraulic diameter $D$ and reference velocity $u_{ref} = \sqrt{\frac{2P_0}{\rho}}$. An estimation of the pressure within the jet $P_j$ yields

$$\frac{P_j}{P_0} = \frac{-2\frac{A_j}{A_2}\left(1 - \frac{A_j}{A_2}\right)}{1 - \frac{2A_j}{A_2}\left(1 - \frac{A_j}{A_2}\right)} \tag{5}$$

and the pressure drop $\Delta P_c = P_c - P_j$ becomes

$$\frac{\Delta P_c}{P_0} = \frac{P_0 - P_j}{P_0}\left(1 - \frac{A_j^2}{A_c^2}\right). \tag{6}$$

The pressure within the constriction is then estimated as $P(0 \leq x \leq L_c) \approx P_j + \frac{x\Delta P_c}{L_c}$ so that the pressure at the center ($x/L_c = 0.5$) of the constriction is approximated as $P_1 \approx P_j + \frac{\Delta P_c}{2}$.

The centerline velocity $u$ within the constriction ($0 \leq x \leq L_c$), *i.e.* in the core flow region outside the boundary layer, is estimated by approximating the area $A(x)$ following (3) and (4) as

$$\frac{A(x)}{A_c} = \left(1 - \frac{2\delta_1(x)}{D}\right)^2 \quad \text{with} \quad \delta_1(x) \approx 1.7\sqrt{\frac{xD}{Re_{ref}}} \tag{7}$$

so that

$$u(x) \approx \frac{\Phi}{A(x)} \tag{8}$$

with volume flow velocity $\Phi$ estimated as

$$\Phi \approx u_{ref} \cdot \bar{A(x)}, \tag{9}$$

where $\bar{A(x)}$ indicates the mean value of $A(x)$ within the constriction using (7). Consequently, flow quantities within the constriction are estimated using a single input parameter (upstream pressure $P_0$) while accounting for the cross-section shape by its hydraulic diameter $D$. Note that downstream from the constriction within the potential core of the jet ($L_c < x \leq x_{pc}$) both the velocity and pressure can be considered constant so that $u(x) \approx \frac{\Phi}{A_j}$ and $P(x) \approx P_j$.

### 3.2. Viscous model

The streamwise momentum equation of the governing Navier–Stokes equation for driving pressure $dP/dx$ is approximated using volume flow velocity conservation $d\Phi/dx = 0$ as [4,5]:

$$-\frac{\Phi^2}{A^3}\frac{dA}{dx} + \frac{1}{\rho}\frac{dP}{dx} = \nu\left(\frac{\partial^2 u}{\partial y^2} + \frac{\partial^2 u}{\partial z^2}\right), \tag{10}$$

with spanwise direction $y$, transverse direction $z$ and velocity $u(x, y, z)$. The flow model expressed in (10) accounts for viscosity (right hand term) as well as flow inertia (first source term at the left hand side) and depends therefore on the area as well as on the shape of the cross-section. It is seen that for a uniform channel, so that $dA/dx = 0$ holds, (10) reduces to purely viscous flow [5,2]. The same way, it is seen that (10) reduces to Euler's equation describing Bernoulli flow when viscosity is neglected, *i.e.* $\nu = 0$ as for an ideal inviscid flow [2].

The pressure distribution $P(x, t)$ as a function of streamwise position $x$ and time $t$ up to flow separation ($x_0 \leq x \leq x_s$) is then given by integration of (10) [5,4] and results in a quadratic equation of volume flow velocity $\Phi$:

$$\begin{aligned} P(x,t) &= P_0 + \frac{1}{2}\rho\Phi^2\left(\frac{1}{A^2(x_0)} - \frac{1}{A^2(x,t)}\right) \\ &\quad + \mu\Phi\int_{x_0}^{x}\frac{dx}{\beta(x,t)}, \qquad \text{if} \quad x_0 \leq x < x_s, \end{aligned} \tag{11}$$

with dynamic viscosity of the fluid $\mu = \rho\nu$ and $\beta$ expressing the viscous contribution to the pressure drop so that it depends on the cross-section shape. The assumption of a stable non-expanding straight jet with infinite potential core extent $x_{pc}^{\infty}$, *i.e.* non-viscous flow, results in $P(x, t) = P_d$ downstream from flow separation ($x \geq x_s$). From (11) is seen that the model adds a viscous correction (last righthand term) to the steady Bernoulli equation [1,2] which relies on the asymptotic expression for fully developed viscous flow.

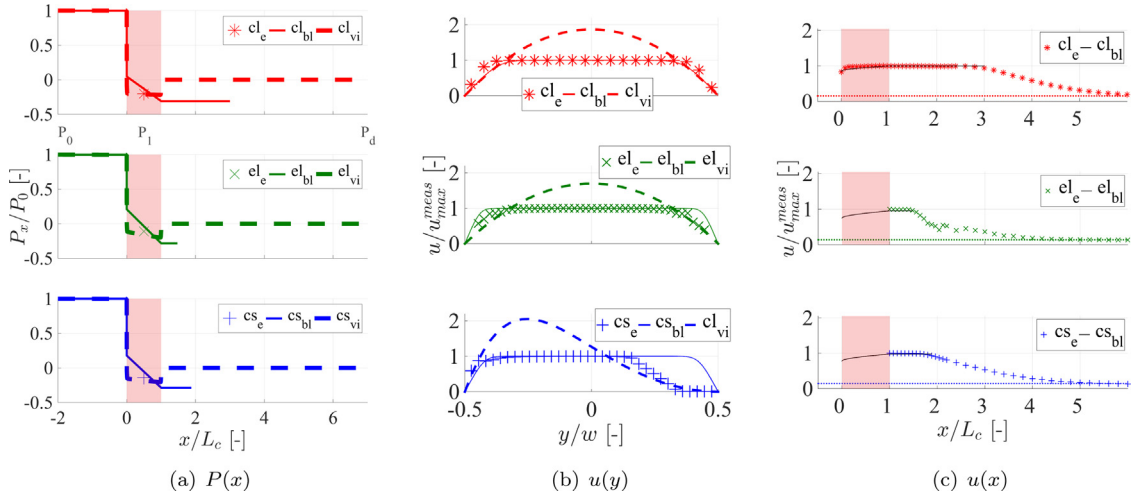


(a) $P(x)$ (b) $u(y)$ (c) $u(x)$

**Fig. 2.** Measured (e – symbol) and modeled (boundary layer model (bl – full line) and viscous model (vi – dashed line) for $P_0 = 35$ Pa for each cross-section shape (circle (cl – top), ellipse (el – middle) and circular sector (cs – bottom)): (a) normalised pressure distribution $P_x/P_0$ and measured pressure $P_1$ at $x/L_c = 0.5$, (b) normalised spanwise velocity profile downstream the constriction $u/u_{\max}^{meas}$ and (c) normalised longitudinal velocity profile $u/u_{\max}^{meas}$. The constricted flow channel portion corresponds to the shaded area.

Therefore (11) is a generalisation of an extensively applied 2D model [6] flow for an arbitrary cross-section shape.

At flow separation ($x = x_s$ and $A = A_s$) $P(x_s, t) = P_d$, so that volume flow velocity $\Phi$ can be estimated from (11) as:

$$\Phi = \left[\mu \int_{x_0}^{x_s} \frac{dx}{\beta(x,t)} + \left\{\left(\mu \int_{x_0}^{x_s} \frac{dx}{\beta(x,t)}\right)^2 + 2(P_0 - P_d)\rho(1/A_s^2 - 1/A^2(x_0))\right\}^{1/2}\right] \times [\rho(1/A_s^2 - 1/A^2(x_0))]^{-1}. \quad (12)$$

Once $\Phi$ is known, $P(x, t)$ along the constricted channel portion is then estimated using (11).

Note that the velocity profile within each cross-section of the channel $u(y, z)$ can be approximated using the streamwise momentum Eq. (10). When applying the no-slip condition ($u = 0$) on the rigid channel walls this can be rewritten as a classical Dirichlet problem which can be solved numerically for an arbitrary cross-section shape or analytically for specific cross-section shapes using *e.g.* separation of variables. Analytical solutions for a given cross-section shape can be written as:

$$u(y, z) = \Phi \frac{\alpha(y, z)}{\beta}, \quad (13)$$

with $\alpha(y, z)$ expressing the velocity-dependence to the spatial position within the cross-section. Concrete expressions of $\beta$ and $\alpha$ for particular cross-section shapes (circular, elliptic and circular sector) are given in Appendix A.

### 3.3. Flow separation model

Pressure recovery is accounted for in the boundary layer model (Section 3.1) so that is reasonable to neglect delayed flow separation ($x_s = x_2 - r_a$ and $A_s = A_c$) when the curvature $r_a$ of the trailing edge of the constriction is small compared to the largest cross-sectional dimension. The viscous model (Section 3.2) does not account for downstream pressure recovery so that a flow separation model is required to account for delayed flow separation and jet formation along the rounded trailing edge of the constriction in order to determine $x_s \geq x_2 - r_a$ and $A_s \geq A_c$. Concretely, an *ad-hoc* geometrical criterion is used to determine the position of jet formation for the viscous model as $A_s = c_s \times A_c$ with $c_s = 1.1$ [6].

**Table 1**
Overview of geometrical parameters (see Figs. 1 and 5).

| | Circle | Ellipse | Circular sector |
|---|---|---|---|
| $D$ [cm] | 1 | 0.67 | 0.72 |
| $w$ [cm] | 1 | 2.24 | 1.73 |
| $h$ [cm] | 1 | 0.45 | 0.9 |

$A_c = 0.79\,\text{cm}^2$, $L_c = 2.5$ cm, $r_a = 0.05$ cm.

This criterion neglects the dependence of the flow separation position on Reynolds number [7,2,1], but its use in combination with a 2D viscous model has been extensively used and validated for the range of Reynolds numbers of interest [6]. Its use allows to focus solely on the influence of the cross-section shape.

## 4. Results

Airflow through a constricted channel (Fig. 1) is considered for three different cross-section shapes (circular, ellipse and circular sector) detailed in Appendix A. Geometrical parameters of each cross-section shape are summarised in Table 1. Constriction length $L_c$ is smaller than the entrance length for each cross-section shape so that boundary layers are developing. The curvature $r_a$ is at least a factor 5 smaller than the largest dimension of the constriction. Analytical solutions obtained using the boundary layer model (Section 3.1) and the viscous model (Section 3.2) are compared to measured values: pressure ($P_1$ at the center of the constriction), longitudinal ($x$-axis) velocity profiles, spanwise ($y$-axis) velocity profiles immediately downstream from the constriction and volume flow velocity $\Phi$ [4]. Dimensions are within the range for which the 2D viscous model is commonly applied. Therefore, although that strictly speaking the viscous model is not applicable since boundary layers are still developing, both model outcomes are compared to experimental data.

Fig. 2 illustrates measured and modeled values or pressure and velocity for $P_0 = 35$Pa for all three cross-section shapes. The modeled pressure distribution along the channel geometry (Fig. 2(a)) shows that the pressure within the constriction decreases as a function of streamwise position for both models although the slope is more steep for the boundary layer (bl) model. Downstream from the constriction the boundary layer model provides a qualitative estimation of the constant pressure profile whereas the viscous (vi) model provides only information within the constriction due

to the erroneous assumption of a straight jet so that the pressure downstream the constriction equals the pressure at the channel exit $P_d = 0$. It is seen that both models provide a good approximation (<10%) of the measured pressure $P_1$ in the middle of the constriction for all assessed cross-section shapes. Consequently, the boundary layer model and the viscous model combined with the *ad-hoc* separation criterion provide an estimation of the pressure distribution within the constriction. The maximum velocity of measured spanwise velocity profiles (Fig. 2(b)) in the core region of the flow corresponds well with values predicted using Blasius' laminar boundary layer profile (<1%) for all assessed cross-section shapes whereas it is overestimated by the viscous model (up to 100%). On the other hand the velocity profile within the boundary layer is captured by the viscous model for all assessed cross-section shapes whereas the boundary layer approach can not predict asymmetrical boundary layer development since only the hydraulic diameter of the cross-section shape is accounted for and not its precise shape. Longitudinal core flow velocity profiles predicted with the boundary layer model are seen to approximate (<5%) measured longitudinal velocity profiles (Fig. 2(c)).

The model outcome within the constriction is then validated for different pressure ratios $P_1/P_0$ and associated volume flow velocities $\Phi$ as a function of bulk Reynolds number $Re = \frac{Du_{b,c}}{\nu}$ with bulk velocity within the constriction $u_{b,c} = \Phi/A_c$. Experimental results show that the cross-section shape influences the pressure ratio up to 10% (Fig. 3(a)) showing the impact of the cross-section shape. The pressure ratio decreases with Reynolds number within the laminar flow regime ($Re \lesssim 7500$). For higher Reynolds number the flow becomes transitional or turbulent so that assessed models are not expected to hold. Measured volume flow velocity $\Phi$ varies up to 20% for $Re \leq 10^4$ as a function of the cross-section shape (Fig. 3(b)).

Modeled and measured values of pressure ratio $P_1/P_0$ and volume flow velocity $\Phi$ as a function of bulk Reynolds number $Re \leq 10^4$ are plotted in Fig. 4. For $4000 \leq Re \leq 7500$ both flow models provide a good estimation (<10%) of the pressure ratio for all cross-section shapes (Fig. 4(a)). In general, it is seen that the boundary layer model and viscous model underestimate and overestimate the pressure drop, respectively. When the Reynolds number decreases the discrepancy between the boundary layer model and measured values increases whereas the discrepancy with the viscous model remains the same. This is partly expected due to the decrease in boundary layer thickness with Reynolds number, so that the viscous model becomes more pertinent and the boundary layer model becomes less suitable. However, it is important to keep in mind that the viscous model predictions rely on the value of the *ad-hoc* separation constant $c_s$ of the used separation model whereas no model constant is used in the boundary layer model. Increasing the separation constant value from $c_s = 1.1$ to $c_s = 1.2$ decreases the pressure ratio with about 20% for all assessed Reynolds numbers. Consequently, the separation constant can be seen as a model tuning parameter whose value depends on the streamwise constriction geometry, *i.e.* in particular the trailing edge curvature, so that it is preferable that measurements are available to set its value. Overall although, the estimation of the pressure ratio with the viscous model is surprisingly accurate given the underlying asymptotic assumption of developed boundary layers. Volume flow velocities

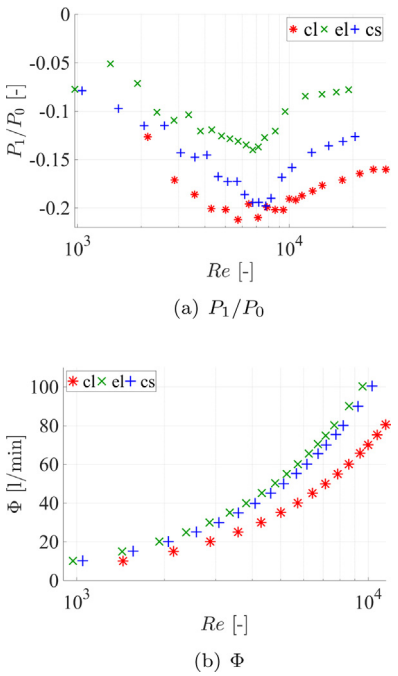


**Fig. 3.** Measured values as a function of bulk Reynolds number $Re$ for each cross-section shape (circle (cl – top), ellipse (el – middle) and circular sector (cs – bottom)): (a) normalised pressure distribution $P_x/P_0$ and (b) volume flow velocity $\Phi$.

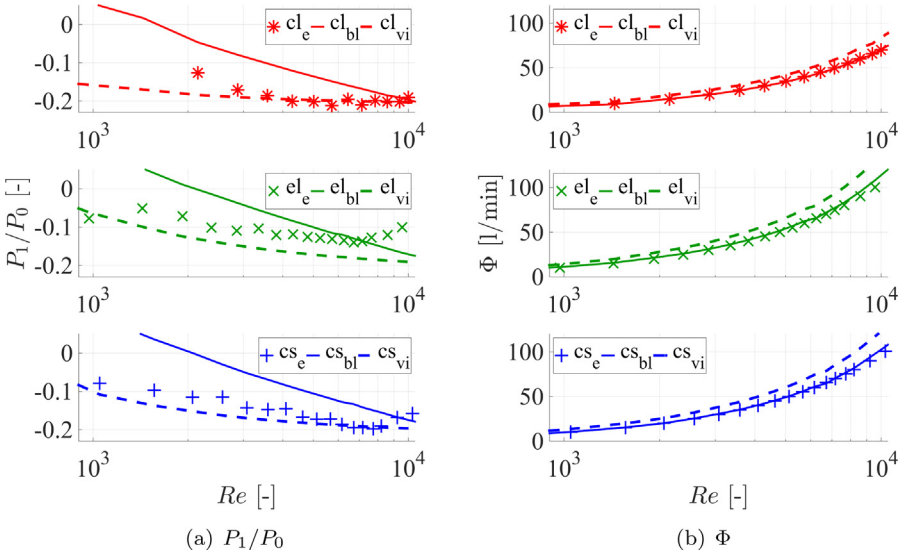


**Fig. 4.** Measured (e – symbol) and modeled (boundary layer model (bl – full line) and viscous model (vi – dashed line) as a function of bulk Reynolds number $Re$ for each cross-section shape (circle (cl – top), ellipse (el – middle) and circular sector (cs – bottom)): (a) normalised pressure distribution $P_x/P_0$ and (b) volume flow velocity $\Phi$.

**Table 2**
$\beta$ and $\alpha$ for cross-section shapes depicted in Fig. 5. Geometrical parameters ($w$, $h$, $A$) depend on streamwise position $x$.

| Shape | $\beta$ | $\alpha(y,z)$ |
|---|---|---|
| Circle | $\frac{A^2}{\pi 8}$ | $\frac{w^2}{4} - \frac{(y^2+z^2)}{4}$ |
| Ellipse | $\frac{w^2A^3}{(\pi^2w^4+16A^2)}$ | $\frac{1}{2}\frac{w^2h^2}{w^2+h^2}\left(1-\frac{y^2}{w^2}-\frac{z^2}{h^2}\right)$ |
| Circular sector[a,b,c] | $\frac{w^4}{4}\left[\frac{\tan 2A/w^2-2A/w^2}{4} - \frac{512A^4}{\pi^5w^8}\sum_{n=1,3,\ldots}^{\infty}\frac{1}{n^2(n+4A/\pi w^2)^2(n-4A/\pi w^2)}\right]$ | $-\frac{1}{4}\left[r^2\left(1-\frac{\cos 2\theta}{\cos\varphi}\right) - \frac{16w^2\varphi^2}{\pi^3}\times\sum_{n=1,3,\ldots}^{\infty}(-1)^{\frac{n+1}{2}}\left(\frac{r}{w}\right)^{\frac{n\pi}{\varphi}}\frac{\cos(n\pi\theta/\varphi)}{n(n+2\varphi/\pi)(n-2\varphi/\pi)}\right]$ |

[a] Infinite sum is limited to $n \leq 60$.
[b] Opening angle $\varphi = 2A/w^2$.
[c] Polar coordinates $(r,\theta)$: $r = \sqrt{y^2+z^2}$ and $\theta = \tan^{-1}\frac{z}{y}$.

estimated from the boundary layer model matches measured values (<10%) whereas estimations resulting from the viscid model overestimate measured Φ-values up to 40% (Fig. 4(b)). This is in agreement with earlier findings related to the spanwise velocity profile (Fig. 2(b)). Indeed, the core flow velocity was overestimated with the viscous model leading to an overestimation of Φ whereas the core flow velocity was estimated accurately with the boundary layer flow model leading to an more accurate estimation of Φ.

## 5. Discussion and conclusion

Two analytical laminar model approaches are proposed which take into account the cross-section shape and viscosity. This way both models can be used as a simple flow model in case the common 2D or axi-symmetrical flow assumption does not hold and information on the cross-section shape is available. For constrictions which are shorter than the entrance length, the boundary layer model can be used. It is shown that it provides a quantitative estimation (<10%) of the pressure within the constricted portion as well as of the volume flow velocity. This model has the advantage that it does not rely on *ad-hoc* model parameters. Furthermore, the boundary layer model provides an analytical model approach available for any cross-section shape since it relies only on the hydraulic diameter, which can *e.g.* be obtained using standard imaging techniques for contour and area detection. Moreover, the core velocity of the flow within the constriction is estimated accurately whereas asymmetries in the velocity profile can not be predicted since only the hydraulic diameter is used to characterise the cross-section shape. It is noted that the accuracy of the viscous model depends on the value of the *ad-hoc* separation constant, which is therefore a crucial model parameter. Furthermore, analytical expressions for the viscous solution are only available for a limited number of cross-section shapes so that an arbitrary cross-section shape requires numerical solution of the Dirichlet problem associated with viscous flow, which excludes this model when a purely analytical approach is sought. Nevertheless, analytical solutions do exist for common shapes, such as the ones assessed here, and the resulting estimation of the pressure within the constricted portion is surprisingly accurate (<10%) since strictly speaking the underlying assumption of fully developed viscous flow does not hold given the length of the constriction. The same assumption of developed viscous flow also leads to an overestimation (40%) of the volume flow velocity and core flow velocity when the viscous model is applied. Nevertheless, it is seen that the velocity in the boundary layers is accurately modeled for all assessed cross-section shapes since the cross-section shape is used as an input parameter, *i.e.* not only its hydraulic diameter. Consequently, when velocity profiles perpendicular to the main flow direction are of interest, both models can be combined to obtain an accurate estimation within the boundary layer and within the core region. Finally, it is noted that the viscous model is of special interest for problems dealing with laminar flow through long channels so that the boundary layers are fully developed such as flow through blood veins.

## Appendix A. Analytical solution of viscous model

Geometrical parameters of particular cross-section shapes (Fig. 5) and associated values of $\beta$ and $\alpha$ (Table 2) of analytical solutions for the viscous model [5] are indicated.

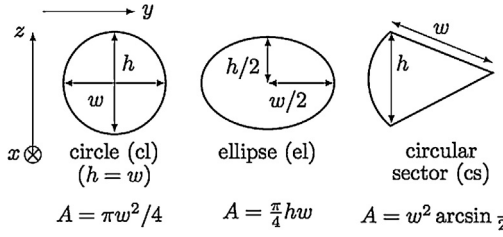


**Fig. 5.** Schematic front view and area $A$ for circle (cl), ellipse (el) and circular sector (cs). Spanwise extent $w$ ($y$-direction) and transverse extent $h$ ($z$-direction) are indicated.

## References

[1] F. White, Viscous Fluid Flow, 2nd ed., McGraw-Hill, New York, 1991.
[2] H. Schlichting, K. Gersten, Boundary Layer Theory, 7th ed., Springer, Berlin, 2000.
[3] S. Naili, M. Thiriet, C. Ribreau, Etude tridimensionnelle des contraintes de cisaillement à la paroi dans un tube de section droite non circulaire, C. R. Mèc. 330 (7) (2002) 483–490.
[4] B. Wu, The Influence of the Cross Section Shape on Channel Flow: Modeling, Simulation and Experiment (Ph.D. thesis), Grenoble University, 2014.
[5] B. Wu, A. Van Hirtum, X. Luo, Pressure driven steady flow in constricted channels of different cross section shapes, Int. J. Appl. Mech. 5 (1) (2013) 1–19.
[6] M. Deverge, X. Pelorson, C. Vilain, P. Lagree, F. Chentouf, J. Willems, A. Hirschberg, Influence of collision on the flow through in-vitro rigid models of the vocal folds, J. Acoust. Soc. Am. 114 (6) (2003) 3354–3362.
[7] A. Van Hirtum, J. Cisonni, X. Pelorson, On quasi-steady laminar flow separation in the upper airways, Commun. Numer. Meth. Engng. 25 (2009) 447–461.